TDA Progress Report 42-104

February 15, 1991

Open-Loop Frequency Acquisition for Suppressed-Carrier Biphase Signals Using One-Pole Arm Filters

B. Shah and J. K. Holmes

Radio Frequency and Microwave Subsystems Section

This article discusses open-loop frequency-acquisition performance for suppressed-carrier binary phase shift keyed signals in terms of the probability of detecting the carrier frequency offset when the arms of the Costas loop detector have one-pole filters. The approach, which does not require symbol timing, uses fast Fourier transforms (FFTs) to detect the carrier frequency offset. The detection probability, which depends on both the 3-dB arm filter bandwidth and the received symbol signal-to-noise ratio, is derived and is shown to be independent of symbol timing. It is shown that the performance of this technique is slightly better than other open-loop acquisition techniques which use integrators in the arms and whose detection performance varies with symbol timing.

I. Introduction

Acquiring and tracking binary phase shift keyed (BPSK) signals in the absence of a residual carrier is one of the many functional requirements that must be met by the Block V receiver [1], the Deep Space Network's (DSN's) next-generation receiver presently under development. The question of how to reduce the frequency error Δf between the received and predicted carrier frequency to within the pull-in range of the Block V receiver's digital Costas loop (the loop used to demodulate BPSK signals) was initially addressed in [2]. The open-loop acquisition techniques discussed in [2] estimate Δf by performing fast Fourier transforms (FFTs) on the phase detector output of Costas-type loops. Because the techniques in [2] use integrate-and-dump arm filters, their performance in terms of probability of detecting Δf depends strongly on symbol timing errors, that is, the receiver's estimate of where a symbol epoch starts and ends. In particular, the performance of these techniques, which worsens with increasing symbol timing errors, motivates evaluating system performance when the integrate-and-dump arm filters are replaced by one-pole arm filters that are independent of symbol timing. This article considers only the estimation of the initial frequency error and does not treat the acquisition of the phase and frequency after the frequency error has been removed and the loop is closed (see Fig. 1). Frequency and phase acquisition when the frequency error is less than one-half the closed-loop noise bandwidth should occur within a few inverse closed-loop noise bandwidths [3,4].

Figure 1 is a functional block diagram of the open-loop frequency-acquisition technique under consideration. The arm filters are assumed to be one-pole filters. The error signal $z'(t)$ is sampled every T sec (T sec is the duration of a symbol), accumulated, and fast-Fourier-transformed to obtain the error signal spectrum. The probability of detecting a tone in white Gaussian noise is well known [5]

and can easily be computed as a function of the error-signal SNR. The results of [5] can be applied in a straightforward manner because, as shown in Appendix A, the error sequence $z(n)$ out of the integrate-and-dump filter is composed of a sinusoid at $2\Delta f$ Hz plus noise which is approximately white and approximately Gaussian. The absolute frequency difference $|2\Delta f|$ can be estimated (it is assumed in the analysis to follow that $\Delta f T \ll 1$) after detecting the error signal in the spectrum at the output of the Costas loop phase detector. Only the absolute value of $2\Delta f$ can be estimated because taking the product of the I and Q arms doubles the frequency error and removes its sign. The sign ambiguity problem can be resolved by offsetting the frequency so that the error Δf always has a known sign.

This article only considers the case of detecting and subsequently estimating the frequency error when the error signal is restricted to a single FFT bin. It also assumes that the error signal is always present. Consequently, the article does not address the question of how to choose a threshold, which is the power level that the FFT bin with the maximum power must exceed before a signal can be declared to be present.

When a tone is known to be present and restricted to a single bin, the maximum likelihood (ML) estimate of the tone is to observe the FFT magnitude spectrum and to select the frequency bin with the maximum power [5]. Note that, in practice, it is unlikely that the error signal will be restricted to a single FFT bin.

In a typical deep-space operation, the Doppler shift is accompanied by a Doppler rate which is removed by ramping the local oscillator phase based on Doppler rate predicts. If the Doppler rate cannot be predicted precisely, the error signal will drift in frequency during the FFT observation time, causing it to smear over multiple bins. Clearly, the extent of the smearing depends on the size of the Doppler rate error. On the other hand, if the Doppler rate is known very accurately so that the signal does not drift appreciably during the observation interval, the signal may be present in multiple bins due to not sampling the discrete-time Fourier transform at its peak (see Chapter 8 of [6]). Restricting the error signal to a single bin greatly simplifies the analysis. Furthermore, it is appropriate because the intent is not to quantify absolute performance but rather to compare performance between the lowpass technique and the integration techniques of [2].

Although other models are not precluded, sampling of $z'(t)$ is modeled as a T-sec integrate-and-dump filter, because doing so defines the signal-to-noise ratio (SNR) of the error sequence $z(n)$ in the same bandwidth as the alternative acquisition techniques studied in [2]. Defining SNRs in the same bandwidth is important when comparing performance between different schemes. Since the arm filters do not require symbol timing, and taking the product of the I and Q arms prior to the integrate-and-dump filter gives rise to a signal component (a tone at $2\Delta f$) whose amplitude does not depend on symbol timing, the performance of the one-pole technique is independent of symbol timing errors. For convenience, the integrator in Fig. 1 is shown as synchronous with symbol transitions although the analysis does not depend on this fact. In fact, the value of integration time T' does not have to be equal to T as long as $\Delta f T' \ll 1$. However, as shown in Section II, performance depends directly on the normalized bandwidth R, defined as the ratio of the 3-dB arm filter bandwidth to the data rate and the symbol SNR.

A mathematical model of the one-pole technique is developed in Section II. Its performance in terms of probability of detecting the frequency difference between the received and predicted carrier frequency is derived in Section III and discussed in Section IV. Conclusions are stated in Section V.

II. Mathematical Model

The received suppressed-carrier BPSK signal, downconverted to an appropriate intermediate frequency (IF), can be modeled as

$$r(t) = \sqrt{2P}d(t)\sin(\omega_i t + \theta_i) + n(t) \tag{1}$$

where P is the received power in watts, ω_i is the IF radian frequency expressed in rad/sec, θ_i is the signal phase in rad, and $d(t)$ is the transmitted data stream given by

$$d(t) = \sum_{k=-\infty}^{+\infty} d_k p(t - kT) \tag{2}$$

where $p(t)$ is the baseband non-return-to-zero (NRZ) pulse limited to T sec and d_k represents the equally likely ± 1 binary symbols. The narrow-band noise process $n(t)$ can be expressed as

$$n(t) = \sqrt{2}n_c(t)\cos(\omega_i t + \theta_i) - \sqrt{2}n_s(t)\sin(\omega_i t + \theta_i) \tag{3}$$

where $n_c(t)$ and $n_s(t)$ are statistically independent stationary band-limited white Gaussian noise processes with one-sided spectral density N_0 watts/Hz and one-sided bandwidth W Hz. The signal $r(t)$ is demodulated by in-phase and quadrature references, $\sqrt{2}\sin(\omega_o t + \theta_o)$ and

$\sqrt{2}\cos(\omega_o t + \theta_o)$, tuned to the predicted carrier frequency and then filtered by a lowpass filter. Neglecting higher frequency terms, the demodulated signals $i(t)$ and $q(t)$ in Fig. 1 can be represented as (see Chapter 5 of [7] for an example):

$$i(t) = Re\left[\sqrt{P}d(t)e^{j\phi}e^{j\Delta\omega t}\right] - Re\left[n_c(t)\frac{1}{j}e^{j\phi}e^{j\Delta\omega t}\right] - Re\left[n_s(t)e^{j\phi}e^{j\Delta\omega t}\right] \quad (4)$$

and

$$q(t) = Re\left[\sqrt{P}d(t)\frac{1}{j}e^{j\phi}e^{j\Delta\omega t}\right] + Re\left[n_c(t)e^{j\phi}e^{j\Delta\omega t}\right] - Re\left[n_s(t)\frac{1}{j}e^{j\phi}e^{j\Delta\omega t}\right] \quad (5)$$

where Re is the real part of a complex number, $\Delta\omega = 2\pi\Delta f$ ($\Delta f \triangleq f_i - f_o$) is the radian frequency error to be estimated, and $\phi \triangleq \theta_i - \theta_o$ is the phase error. Let $D(\omega)$, $N_s(\omega)$, and $N_c(\omega)$ be the Fourier transforms of the baseband signals $d(t)$, $n_s(t)$, and $n_c(t)$. Then the Fourier representations of $i(t)$ and $q(t)$ are given by

$$I(\omega) = \frac{\sqrt{P}}{2}\left[D(\omega-\Delta\omega)e^{j\phi} + D^*(-\omega-\Delta\omega)e^{-j\phi}\right] - \frac{1}{2j}\left[N_c(\omega-\Delta\omega)e^{j\phi} - N_c^*(-\omega-\Delta\omega)e^{-j\phi}\right] - \frac{1}{2}\left[N_s(\omega-\Delta\omega)e^{j\phi} + N_s^*(-\omega-\Delta\omega)e^{-j\phi}\right] \quad (6)$$

and

$$Q(\omega) = \frac{\sqrt{P}}{2j}\left[D(\omega-\Delta\omega)e^{j\phi} - D^*(-\omega-\Delta\omega)e^{-j\phi}\right] + \frac{1}{2}\left[N_c(\omega-\Delta\omega)e^{j\phi} + N_c^*(-\omega-\Delta\omega)e^{-j\phi}\right] - \frac{1}{2j}\left[N_s(\omega-\Delta\omega)e^{j\phi} - N_s^*(-\omega-\Delta\omega)e^{-j\phi}\right] \quad (7)$$

where X^* is the conjugate of the complex number X. Let $H(\omega)$ be the transfer function of the arm filters in Fig. 1. Then, the filter outputs in the inphase and quadrature arms are given as

$$Z_i(\omega) = \sqrt{\frac{P}{2}}\left[\tilde{D}(\omega-\Delta\omega)e^{j\phi} + \tilde{D}^*(-\omega-\Delta\omega)e^{-j\phi}\right] - \frac{1}{2j}\left[\tilde{N}_c(\omega-\Delta\omega)e^{j\phi} - \tilde{N}_c{}^*(-\omega-\Delta\omega)e^{-j\phi}\right] - \frac{1}{2}\left[\tilde{N}_s(\omega-\Delta\omega)e^{j\phi} + \tilde{N}_s{}^*(-\omega-\Delta\omega)e^{-j\phi}\right] \quad (8)$$

and

$$Z_q(\omega) = \frac{\sqrt{P}}{2j}\left[\tilde{D}(\omega-\Delta\omega)e^{j\phi} - \tilde{D}^*(-\omega-\Delta\omega)e^{-j\phi}\right] + \frac{1}{2}\left[\tilde{N}_c(\omega-\Delta\omega)e^{j\phi} + \tilde{N}_c{}^*(-\omega-\Delta\omega)e^{-j\phi}\right] - \frac{1}{2j}\left[\tilde{N}_s(\omega-\Delta\omega)e^{j\phi} - \tilde{N}_s{}^*(-\omega-\Delta\omega)e^{-j\phi}\right] \quad (9)$$

where $\tilde{D}(\omega)$, $\tilde{N}_c(\omega)$, and $\tilde{N}_s(\omega)$ are defined, as in [7], as

$$\tilde{D}(\omega) = D(\omega)H(\omega+\Delta\omega) \quad (10)$$

$$\tilde{N}_c(\omega) = N_c(\omega)H(\omega) \quad (11)$$

$$\tilde{N}_s(\omega) = N_s(\omega)H(\omega) \quad (12)$$

Equations (8) and (9) represent the output of the arm filters when the signal portion of the input has bandpass spectra centered at $\Delta\omega$, and the input noise is bandlimited white noise with bandwidth $W \gg B + \Delta f$ where B Hz is the 3-dB bandwidth of $H(\omega)$. Equations (8) and (9) are applicable since the demodulated signals $i(t)$ and $q(t)$ have signal spectra centered at $\Delta\omega$ during acquisition. The time-domain representations of $Z_i(\omega)$ and $Z_q(\omega)$ are given by

$$z_i(t) = Re\left[\sqrt{P}\tilde{d}(t)e^{j\phi}e^{j\Delta\omega t}\right] + \tilde{n}_i(t) \quad (13)$$

and

$$z_q(t) = Re\left[\sqrt{P}\tilde{d}(t)\frac{1}{j}e^{j\phi}e^{j\Delta\omega t}\right] + \tilde{n}_q(t) \quad (14)$$

where

$$\tilde{n_i}(t) = -Re\left[\tilde{n_c}(t)\frac{1}{j}e^{j\phi}e^{j\Delta\omega t}\right]$$

$$- Re\left[\tilde{n_s}(t)e^{j\phi}e^{j\Delta\omega t}\right] \quad (15)$$

$$\tilde{n_q}(t) = Re\left[\tilde{n_c}(t)e^{j\phi}e^{j\Delta\omega t}\right]$$

$$- Re\left[\tilde{n_s}(t)\frac{1}{j}e^{j\phi}e^{j\Delta\omega t}\right] \quad (16)$$

and where $\tilde{d}(t)$, $\tilde{n_s}(t)$, and $\tilde{n_c}(t)$ are the inverse Fourier transforms of $\tilde{D}(\omega)$, $\tilde{N_s}(t)$, and $\tilde{N_c}(t)$. It can be shown from Eq. (10) that when $\Delta\omega \neq 0$, $\tilde{d}(t)$ is in general complex; when $\Delta\omega = 0$, it is real.

III. One-Pole Arm Filters

Assuming that the arm filters in Fig. 1 are one-pole filters with 3-dB bandwidth B Hz, the transfer function $H(\omega)$ is given by

$$H(\omega) = \frac{\omega_B}{j\omega + \omega_B} \quad (17)$$

where $\omega_B = 2\pi B$ is the 3-dB filter bandwidth in radians. For such a filter, the error signal $z'(t) = z_i(t)z_q(t)$ can be computed as (see Appendix A):

$$z'(t) = A(P, \Delta\omega T, R)\sin(2\Delta\omega t + 2\phi + \xi) + n'_{eff}(t) \quad (18)$$

The amplitude A given by Eq. (A-5) is a function of many variables, including the normalized bandwidth $R = BT$, which is the ratio of the 3-dB bandwidth of the one-pole filter to the data rate $R_s = 1/T$. It can be shown that A does not change significantly with ΔfT when $\Delta fT \ll 1$. Since this article only considers the case $\Delta fT \ll 1$, the dependence of A on $\Delta\omega T$ is omitted in subsequent expressions to allow a simpler notation. Since the interest here is the magnitude of the error signal, the phase ξ in Eq. (18) is not relevant and consequently is not included here. The effective noise $n'_{eff}(t)$ into the integrator is defined as

$$n'_{eff}(t) \triangleq n'_{ss}(t) + n'_{sn}(t) + n'_{nn}(t) \quad (19)$$

where the self-noise due to the signal times the signal product, $n'_{ss}(t)$, is given by Eq. (A-7); the noise due to the signal times the noise product, $n'_{sn}(t)$, is given by Eq. (A-8); and the noise due to the noise times the noise product, $n'_{nn}(t)$, is given by Eq. (A-9). The signal–signal noise, $n'_{ss}(t)$, which is a consequence of intersymbol interference (ISI), has two terms. The first term has a continuous spectrum and zero mean, whereas the second term gives rise to line spectra at harmonics (not including the fundamental harmonic) of the symbol rate. The noise $n'_{sn}(t)$ is the lowpass filtered signal response at time t (due to the present as well as previously transmitted pulses) times the thermal noise filtered by a lowpass filter. Lastly, the noise–noise process $n'_{nn}(t)$ is the product of the filtered thermal noise in the inphase arm and the quadrature-phase arm.

These noises are independent of each other since data and noise are assumed to be independent. Consequently, the average power of the effective noise is the sum of the average power of each of the noise processes above. Expressions for average noise power are given by evaluating the autocorrelation functions of Eqs. (A-11) through (A-13) at $\tau = 0$.

Referring to Fig. 1, the process $z'(t)$ is integrated and dumped to obtain the sequence $z(n)$. Assuming that the frequency error is much smaller than the data rate, that is, $\Delta fT \ll 1$, it is shown in Eq. (A-15) that the error sequence $z(n)$ can be represented as

$$z(n) = A(P, R)\sin[2\Delta\omega(nT + T/2) + 2\phi + \xi] + n_{eff}(n) \quad (20)$$

where $A(P, R)$ is as defined in Eq. (A-5) and the effective noise sequence $n_{eff}(n)$ is defined to be

$$n_{eff}(n) \triangleq n_{ss}(n) + n_{sn}(n) + n_{nn}(n) \quad (21)$$

where the noises $n_{ss}(n)$, $n_{sn}(n)$, and $n_{nn}(n)$ are given by Eqs. (A-16) through (A-18). The discrete autocorrelation functions of these noises, assuming $\Delta\omega = 0$, are derived in Appendix C and listed in Eqs. (A-19) through (A-21). These functions are exact except for the autocorrelation of $n_{ss}(n)$, which neglects the negligible second term in Eq. (A-7). Since data and noise are independent, the effective noise power is given as σ^2_{eff}, where

$$\sigma^2_{eff} = \sigma^2_{ss} + \sigma^2_{sn} + \sigma^2_{nn} \quad (22)$$

and where Eqs. (A-19) through (A-21) for $R_{ss}(m)$, $R_{sn}(m)$, and $R_{nn}(m)$ yield

$$\sigma^2_{ss} = \frac{P^2}{8\pi^2R^2}\left(-1 + \frac{e^{-2\pi R} + e^{2\pi R}}{2}\right)^2\left(\frac{e^{-4\pi R}}{1 - e^{-4\pi R}}\right) \quad (23)$$

$$\sigma_{sn}^2 = P\sigma^2\left[1 - \frac{1}{4\pi R}\left(5 - \frac{9}{4\pi R}\right)\right.$$

$$+ \frac{e^{-2\pi R}}{4}\left(1 + \frac{1}{2\pi R} - \frac{17}{8\pi^2 R^2}\right)$$

$$\left. - \frac{1}{16\pi^2 R^2}\left(e^{-4\pi R} + \frac{e^{-6\pi R}}{2}\right)\right] \quad (24)$$

$$\sigma_{nn}^2 = \sigma^4\left[\frac{\pi R}{2} - \frac{1}{8}(1 - e^{-4\pi R})\right] \quad (25)$$

where $\sigma^2 = N_0/2T$. The signal-to-noise ratio of the error sequence $z(n)$, defined as signal power divided by the noise power, is given by

$$SNR_z(R) = \frac{A^2(P,R)}{2\sigma_{eff}^2} \quad (26)$$

where, after one uses Eq. (A-5) for $A(P,R)$ and Eq. (22) for σ_{eff}, the term SNR_z can be written in terms of the received symbol SNR as

$$SNR_z(R) = \frac{|C_0(R)|^2}{8C_{ss}(R) + \frac{4}{SNR}C_{sn}(R) + \frac{2}{SNR^2}C_{nn}(R)} \quad (27)$$

where SNR $\triangleq PT/N_0$, $|C_0(R)|^2$ is given by Eq. (A-6), and where $C_{ss}(R) = \sigma_{ss}^2/P^2$, $C_{sn}(R) = \sigma_{sn}^2/P\sigma^2$, and $C_{nn}(R) = \sigma_{nn}^2/\sigma^4$. The quantities $C_{ss}(R)$, $C_{sn}(R)$, and $C_{nn}(R)$ depend on R because σ_{ss}^2, σ_{sn}^2, and σ_{nn}^2 are functions of R.

As expected, for a given SNR, SNR_z is primarily a function of R. Equation (27) is exact except for $C_{ss}(R)$, which is approximate because σ_{ss}^2 is an approximation: see derivation of Eq. (A-19). Although it is not proven, the σ_{ss}^2 given by Eq. (23) is believed to be a slight upper bound to the self-noise power for NRZ pulses. At symbol SNRs below 0 dB, SNR_z is a very accurate expression for the true error sequence SNR. This is because in this region the sum of $C_{sn}(R)$ and $C_{nn}(R)$, which are scaled by the inverse of SNR and are exact, dominates $C_{ss}(R)$. For SNRs above 0 dB, SNR_z is believed to be a slight lower bound to the true error sequence SNR, because in this case $C_{ss}(R)$ dominates the other two terms in the denominator of Eq. (27).

The objective of the analysis presented here is to enable the designer to choose an arm filter bandwidth R for this scheme that optimizes the probability of detecting a tone in white Gaussian noise, that is, detecting the frequency error between the incoming signal and the local oscillator frequency so that the reference frequency can be moved to the input frequency. Then the loop can be closed to speed acquisition. This is accomplished by choosing an R that optimizes the SNR of a tone in white Gaussian noise. The error sequence SNR given by Eq. (27) represents the SNR of a tone imbedded in noise $n_{eff}(n)$, which is neither exactly white nor exactly Gaussian but can be assumed to be both in practice. This is because the random variable in each FFT bin, which results from summing N appropriately weighted random variables at the FFT input, tends toward a Gaussian random variable for large values of N. The correlation coefficient ρ for a one-symbol separation is less than 0.2 for symbol SNRs below 0 dB and $R > 0.3$. When $\rho \leq 0.2$, the assumption of independent samples out of the integrate-and-dump is valid. Also, it is true that $n_{eff}(n)$ is essentially white when $R > 0.5$ for SNRs above 0 dB. Thus, for any optimum R it is essentially true that the integrate-and-dump output sequence is white and so the results of [5] apply for the probability of correct detection of the frequency error.

IV. Numerical Results and Discussion

A. SNR Degradation

Figure 2 depicts SNR degradation D versus normalized bandwidth R. Degradation is defined as the reduced error signal SNR given by Eq. (26) relative to the SNR of the error signal of an "ideal" Costas loop. An ideal Costas loop has integrate-and-dump arm filters with (magically) perfect symbol timing instead of lowpass filters. In [2] it is shown that the error signal SNR for an ideal Costas loop detector SNR_i is given by

$$SNR_i = \frac{SNR}{4 + 2/SNR} \quad (28)$$

where $SNR \triangleq PT/N_0$ is the received symbol signal-to-noise ratio. In mathematical terms, the degradation is given as

$$D(R) = \frac{SNR_i}{SNR_z(R)} \quad (29)$$

Note that degradation defined in this way is a number greater than one, which indicates an actual loss. Figures 2(a) through 2(e) show degradation $D(R)$ versus a relative 3-dB bandwidth R for various values of SNR. As

expected, there is an optimum value for R (i.e., arm filter bandwidth) that minimizes degradation and thus maximizes error signal SNR. Values of R greater or less than this optimum value decrease error signal SNR because they increase the noise power faster than the error signal power. From Fig. 2 it is clear that lower symbol SNRs result in smaller optimum R values.

The reference SNR, SNR_i given by Eq. (28), is plotted versus symbol SNR in Fig. 3. Figures 3 and 2 relate received symbol SNR to the error signal SNR, SNR_z.

B. Probability of Detection

The outlier probability (missed detection probability) q, defined as the probability that the magnitude of any FFT noise-only bin exceeds the magnitude of the signal-plus-noise bin, is given by $q = 1 - p$, where p, the probability of detecting the correct frequency offset, is given by ($M = N/2$):

$$p = \int_0^\infty 2M(SNR_z)ye^{-M(SNR_z)(y^2+1)} \times I_0\left[2My(SNR_z)\right]\left[1 - y^2e^{-M(SNR_z)}\right]^M dy \tag{30}$$

where N is the FFT size (and M is one-half the FFT size) and $I_0()$ is the modified Bessel function of the first kind. Thus, this probability for p is given by [5] except that the factor of $M - 1$ is replaced by M in the last bracketed term. If M were $M - 1$, the expressions in [5] and Eq. (30) would be identical. The results in [5] are slightly different from Eq. (30) because the results in [5] are derived for the more general complex FFT case. Figure 4 depicts q versus SNR where SNR corresponds to the signal-to-noise ratio at the FFT input (i.e., SNR_z). Figure 4 applies only when the noise prior to the FFT operation is white and Gaussian. In the case described here, the error signal noise component $n_{eff}(n)$ is essentially white and Gaussian. Since the N-point FFT has input samples at the symbol rate, the frequency bin size is

$$\Delta f_{BIN} = \frac{1}{NT} \tag{31}$$

with $(1/T)$ as the integrate-and-dump rate which is assumed to be the symbol rate in this analysis in order to compare the results with [2]. Thus, when the correct frequency bin is detected, the actual frequency error, assuming that the error signal is at the center of a bin, is reduced to a maximum of $\Delta f_{BIN}/2$. As long as the maximum frequency error is less than one-half of the loop bandwidth (that is, N is large enough), and

$$\frac{\Delta f_{BIN}}{2} \leq \frac{B_L}{2} \tag{32}$$

or equivalently

$$\Delta f_{BIN} \leq B_L \tag{33}$$

where B_L is the one-sided (closed-loop) bandwidth of the Costas loop, the frequency and phase pull-in should be on the order of a few inverse B_L's.

The following example illustrates how to use the curves presented in this section to compute the probability of correctly detecting the frequency error "seen" by the loop. Suppose that the received symbol SNR is 0 dB. Then, from Fig. 3, the error signal SNR of an ideal Costas loop is -11 dB. Assuming that $R = 0.3$, from Fig. 2(c), $D(0.3) = 0.3$ dB and the error signal SNR $SNR_z = -11.3$ dB. Finally, from Fig. 4, the probability of incorrectly detecting the actual frequency error for a 1024-point FFT is 1.3×10^{-6}.

V. Conclusion

This article has described a method of determining the probability of correctly identifying the frequency error between the incoming suppressed-carrier signal and the frequency of the Costas loop oscillator in order to aid in the frequency acquisition of the suppressed-carrier signal. The detector chosen for estimating the frequency error is the error detector of the Costas loop, which is used for tracking the suppressed-carrier signal. The error signal is not fed back to the loop filter and numerically controlled oscillator (NCO), but rather sent to an N-point FFT. The FFT then estimates the frequency error, the Costas loop is closed, and the loop NCO is adjusted in frequency to reduce the initial frequency error to a very small value.

Knowing the symbol SNR allows the determination of the SNR_i and, from Figs. 2(a) through 2(e), the additional degradation D. The addition of these two terms yields SNR_z, which is the abscissa entry on the plot of the probability of incorrectly detecting the actual frequency error (Fig. 4). One minus this probability yields the probability of correctly detecting the initial frequency error between the received signal and the rest frequency of the Costas loop NCO.

This scheme compares favorably to the three methods suggested in [2]. In particular, at SNRs that are ≤ 0 dB, the staggered approach of [2] is best (minimum degradation). Comparing the average loss (averaged over timing error) at SNRs ≤ 0 dB, the one-pole arm filter approach is about 0.5 dB better. At SNRs ≥ 0 dB it is better by more than 0.5 dB.

Whether the one-pole filter approach or one of the methods suggested in [2] will be used for the Block V receiver depends on hardware considerations, since the performance of the best integrate-and-dump arm filter technique is nearly comparable to the one-pole arm filter approach and is easily switched to the optimum tracking configuration with integrate-and-dump arm filters.

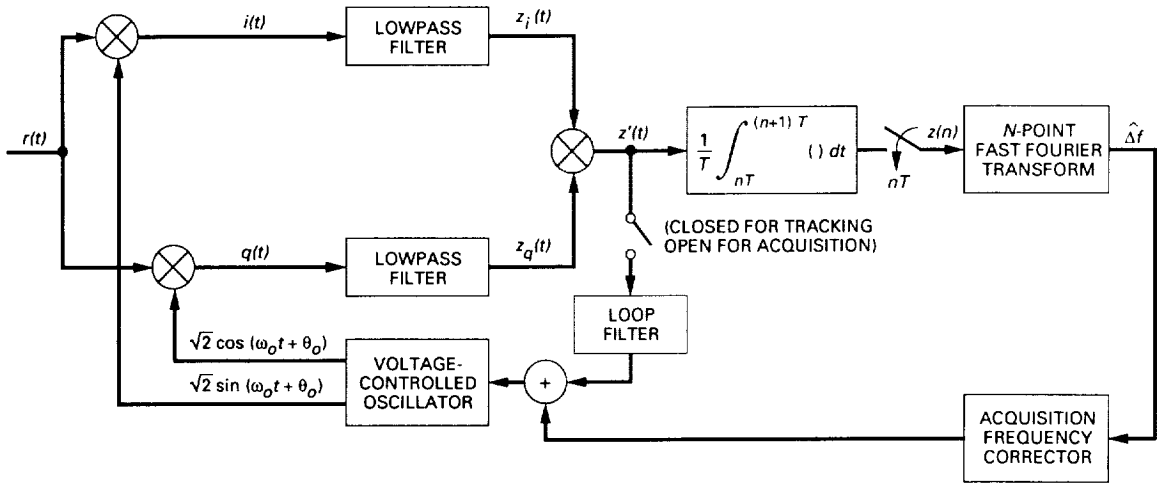

Fig. 1. Costas loop error detector to determine and correct the frequency error between the input and the reference oscillators.

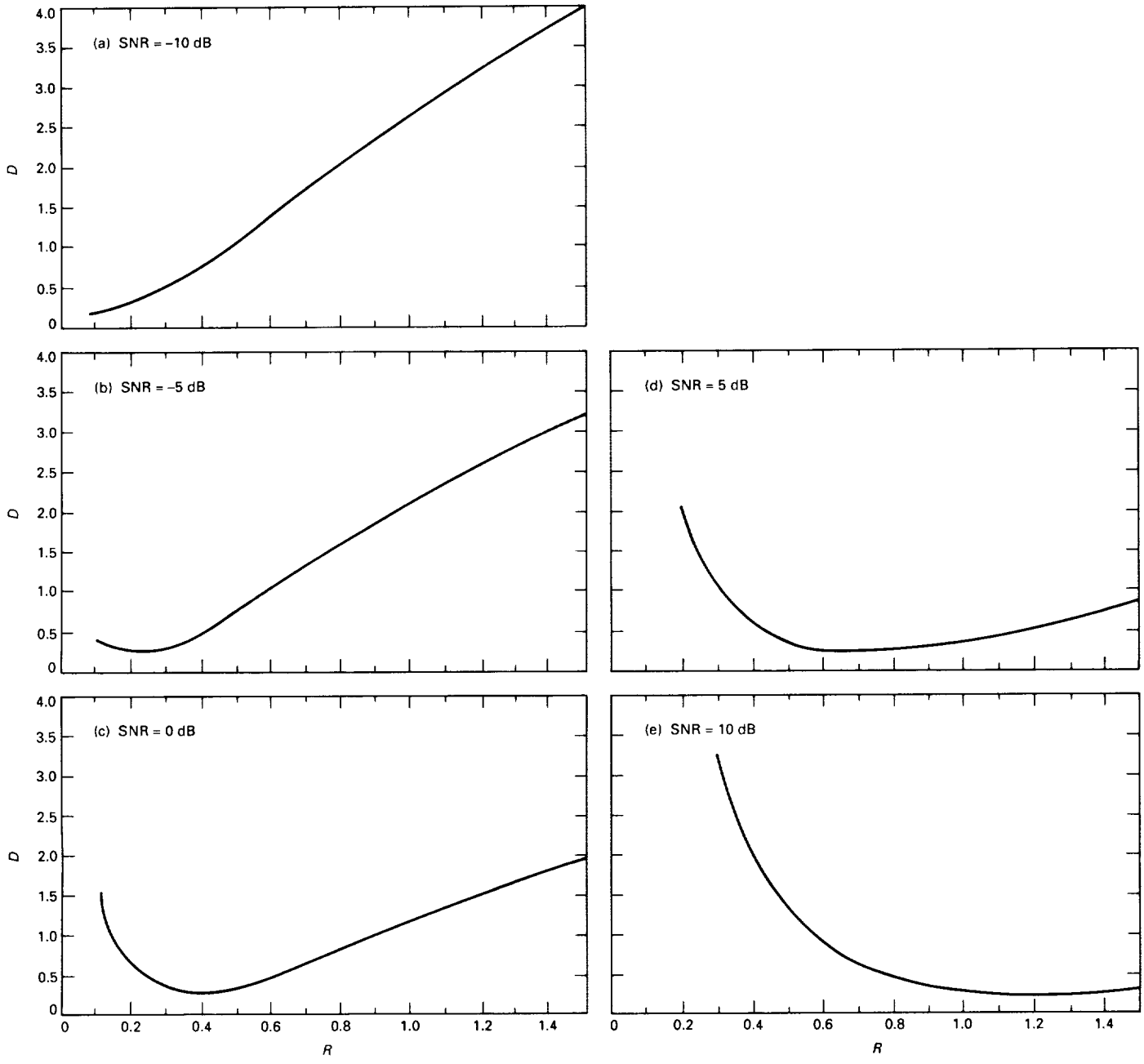

Fig. 2. Signal-to-noise degradation D versus normalized bandwidth R for $0 \leq \Delta\omega T \leq 0.1$ and for various values of SNR.

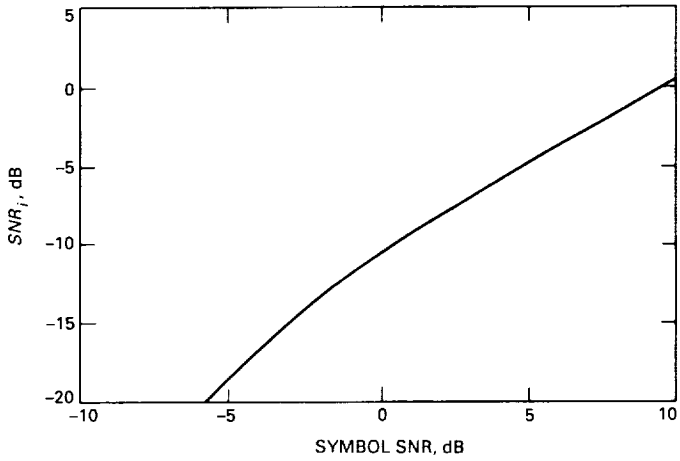

Fig. 3. Signal-to-noise ratio of the "ideal" integrate-and-dump Costas detector versus symbol SNR.

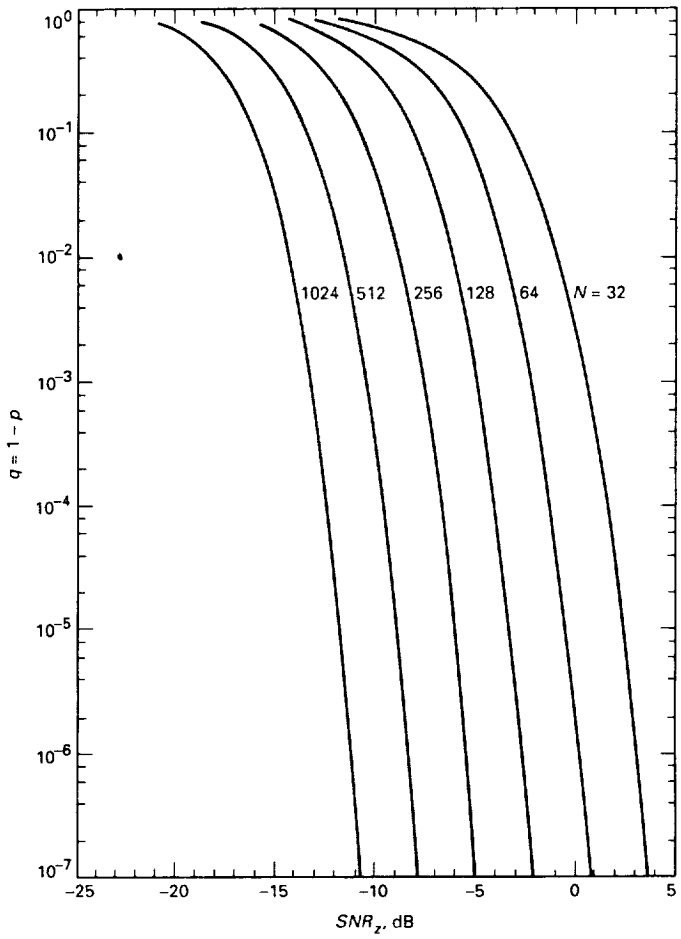

Fig. 4. Probability of incorrectly detecting the frequency error with a Costas loop error detector.

Appendix A

Derivation of the Error Sequence *z(n)*

Figure 1 shows how lowpass filtered signals are collapsed into an error signal that can be Fourier transformed to estimate the frequency error Δf. The received signal $r(t)$ downconverted to an appropriate IF is given by Eqs. (1)-(3). The signal $r(t)$ is first demodulated and then lowpass filtered to produce the functions $z_i(t)$ and $z_q(t)$, which are given by Eqs. (13) and (14). Referring to Fig. 1, the error signal $z'(t)$ is given by

$$\begin{aligned} z'(t) &= z_i(t)z_q(t) \\ &= Im\left[\frac{P}{2}\tilde{d}^2(t)e^{j2(\Delta\omega t+\phi)}\right] + Re\left[\sqrt{P}\tilde{d}(t)e^{j(\Delta\omega t+\phi)}\right]\tilde{n}_q(t) + Re\left[\sqrt{P}\tilde{d}(t)\frac{1}{j}e^{j(\Delta\omega t+\phi)}\right]\tilde{n}_i(t) + \tilde{n}_i(t)\tilde{n}_q(t) \end{aligned} \tag{A-1}$$

where Re and Im are, respectively, the real and imaginary parts of a complex number, and where $\tilde{n}_i(t)$ and $\tilde{n}_q(t)$ are given by Eqs. (15) and (16). The quantity $\tilde{d}^2(t)$ is given as

$$\tilde{d}^2(t) = \left|\tilde{d}^2(t)\right| e^{j\xi(t)} \tag{A-2}$$

It can be shown from Eq. (10) that $\tilde{d}^2(t)$, which is generally a complex quantity, reduces to a real quantity when $\Delta\omega = 0$. In this case, Eq. (A-1) reduces to $(P\tilde{d}^2(t)/2)\sin 2\phi$ plus noise. This is the well-known form for the error signal of a Costas loop [8], where the quantity $\tilde{d}(t)$ is the filtered version of the baseband data $d(t)$. When $\Delta\omega \neq 0$, the function $\tilde{d}^2(t)$ for a one-pole filter is derived in Appendix B to be

$$\tilde{d}^2(t) = \sum_{n=-\infty}^{\infty} C_n(R)e^{j(2n\pi t/T)} + \sum_{k=-\infty}^{\infty}\sum_{\substack{l=-\infty \\ l\neq k}}^{\infty} d_k d_l \tilde{p}(t-lT)\tilde{p}(t-kT) \tag{A-3}$$

where $\tilde{p}(t)$ and $C_n(R)$ are respectively given by Eqs. (B-8) and (B-9). Using Eq. (A-3) for $\tilde{d}^2(t)$ and Eq. (B-4) for $\tilde{d}(t)$ in Eq. (A-1), the error signal can be written as

$$z'(t) = A(P,R)\sin(2\Delta\omega t + 2\phi + \xi) + n'_{eff}(t) \tag{A-4}$$

where

$$A(P,R) = \frac{P}{2}|C_0(R)| \tag{A-5}$$

and where, from Eq. (B-10), the squared magnitude of $C_0(R)$ can be computed to be

$$\begin{aligned} |C_0(R)|^2 = \left[\frac{1}{1+\left(\frac{\Delta\omega T}{2\pi R}\right)^2}\right]^2 \Bigg\{ 1 + \frac{1}{1+\left(\frac{\Delta\omega T}{2\pi R}\right)^2}\Bigg[\frac{1}{(2\pi R)^2}\left(1+e^{-4\pi R}-2e^{-2\pi R}\cos(\Delta\omega T)\right) \\ - \frac{2}{2\pi R}\left(1-e^{-2\pi R}\left(\cos(\Delta\omega T) - \frac{\Delta\omega T}{2\pi R}\sin(\Delta\omega T)\right)\right)\Bigg]\Bigg\} \end{aligned} \tag{A-6}$$

Since the interest here is in the spectrum of the error signal, the phase ξ in Eq. (A-4) is not relevant. Consequently, it is not included here.

The effective noise $n'_{eff}(t)$ in Eq. (A-4) is defined in Eq. (19), where

$$n'_{ss}(t) = Im\left[\frac{P}{2}\sum_{k=-\infty}^{\infty}\sum_{\substack{l=-\infty \\ l\neq k}}^{\infty} d_k d_l \tilde{p}(t-kT)\tilde{p}(t-lT)e^{j2(\Delta\omega t+\phi)}\right] + Im\left[\frac{P}{2}\sum_{\substack{n=-\infty \\ n\neq 0}}^{\infty} C_n(R)e^{j(2n\pi t/T)}e^{j2(\Delta\omega t+\phi)}\right] \tag{A-7}$$

$$n'_{sn}(t) = Re\left[\sqrt{P}\sum_{k=-\infty}^{\infty} d_k \tilde{p}(t-kT)e^{j(\Delta\omega t+\phi)}\right]\tilde{n_q}(t) + Re\left[\sqrt{P}\sum_{k=-\infty}^{\infty} d_k \tilde{p}(t-kT)\frac{1}{j}e^{j(\Delta\omega t+\phi)}\right]\tilde{n_i}(t) \tag{A-8}$$

$$n'_{nn}(t) = \tilde{n_i}(t)\tilde{n_q}(t) \tag{A-9}$$

where the binary symbols d_k are ± 1 at random with probability one-half, $\tilde{p}(t)$ and $C_n(R)$ are given by Eqs. (B-8) and (B-9), and $\tilde{n_i}(t)$ and $\tilde{n_q}(t)$ are given by Eqs. (15) and (16). These noises are independent of one another since data and noise are assumed to be independent. Consequently, the autocorrelation of the effective noise is the sum of the autocorrelation of each of the noises. Mathematically,

$$R'_{eff}(\tau) = R'_{ss}(\tau) + R'_{sn}(\tau) + R'_{nn}(\tau) \tag{A-10}$$

where, from Appendix C,

$$R'_{ss}(\tau) \approx \frac{P^2T}{8\pi^2R^2}\left(-1+\frac{e^{-2\pi R}+e^{2\pi R}}{2}\right)^2\left(\frac{e^{-4\pi R}}{1-e^{-4\pi R}}\right)\delta(\tau) \tag{A-11}$$

$$R'_{sn}(\tau) = \begin{cases} \frac{P}{2}\left[2\left(1-\frac{|\tau|}{T}\right) - \frac{e^{-2\pi B|\tau|}}{2\pi R}\left(2-e^{-2\pi R}\right) + \frac{e^{2\pi B|\tau|}}{2\pi R}e^{-2\pi R}\right]\frac{N_0}{2}\pi B e^{-2\pi B|\tau|}, & |\tau| \leq T \\ -\frac{P}{2}\frac{e^{-2\pi B|\tau|}}{2\pi R}\left(2-e^{-2\pi R}-e^{2\pi R}\right)\frac{N_0}{2}\pi B e^{-2\pi B|\tau|}, & |\tau| \geq T \end{cases} \tag{A-12}$$

$$R'_{nn}(\tau) = \left(\frac{N_0}{2}\pi B\right)^2 e^{-4\pi B|\tau|} \tag{A-13}$$

The preceding equations describe the second-order statistics of the noise, which is usually fed back to close the loop along with the signal component. Consequently, the equations can be used to compute the tracking variance of a Costas loop with one-pole arm filters. The tracking variance was computed (in the absence of self-noise) by using the noise statistics above. It was found to be the same as that computed in Chapter 5 of [7]. Although this is not a definitive test of the accuracy of the equations above, it certainly enhances confidence in them.

As shown in Fig. 1, the error signal $z'(t)$ is integrated and dumped every T sec to obtain the error sequence $z(n)$. That is,

$$z(n) = \frac{1}{T}\int_{nT}^{(n+1)T} z'(t)dt \tag{A-14}$$

Assuming that the frequency error to be estimated, Δf, is small relative to the data rate, $R_s = 1/T$, allows one to write $z(n)$ as

$$z(n) = A(P,R)\sin[2\Delta\omega(nT + T/2) + 2\phi + \xi] + n_{eff}(n) \tag{A-15}$$

where the sinusoids in Eq. (A-4), which are approximately constant over T sec by assumption, can be removed outside the integral after evaluating them at the midpoint of the integration window. The amplitude $A(P,R)$ is given by Eq. (A-5), the phase ξ is not computed because it is not relevant, and the effective noise $n_{eff}(n)$ is given by Eq. (21), where

$$n_{ss}(n) = \frac{1}{T}\int_{nT}^{(n+1)T} n'_{ss}(t)dt \tag{A-16}$$

$$n_{sn}(n) = \frac{1}{T}\int_{nT}^{(n+1)T} n'_{sn}(t)dt \tag{A-17}$$

$$n_{nn}(n) = \frac{1}{T}\int_{nT}^{(n+1)T} n'_{nn}(t)dt \tag{A-18}$$

where $n'_{ss}(t)$, $n'_{sn}(t)$, and $n'_{nn}(t)$ are given by Eqs. (A-7) through (A-9). The discrete autocorrelation functions of the noises above, which are computed in Appendix C, are

$$R_{ss}(m) = \begin{cases} \dfrac{P^2}{8\pi^2R^2}\left(-1 + \dfrac{e^{-2\pi R} + e^{2\pi R}}{2}\right)^2 \dfrac{e^{-4\pi R}}{1 - e^{-4\pi R}}, & m = 0 \\ 0, & m \neq 0 \end{cases} \tag{A-19}$$

$$R_{sn}(m) = \begin{cases} P\sigma^2\left[1 - \frac{1}{2\pi R}\left(\frac{5}{2} - \frac{9}{8\pi R}\right) + e^{-2\pi R}\left(\frac{1}{4} + \frac{1}{4(2\pi R)} - \frac{17}{8(2\pi R)^2}\right) - \frac{e^{-4\pi R}}{4(2\pi R)^2} + \frac{e^{-6\pi R}}{8(2\pi R)^2}\right], & m = 0 \\ P\sigma^2\left[\frac{1}{4\pi R}\left(1 - \frac{9}{8\pi R}\right) + \frac{e^{-2\pi R}}{8}\left(1 + \frac{5}{2\pi R} + \frac{9}{4\pi^2R^2}\right) - \frac{1}{8\pi R}\left(1 + \frac{1}{8\pi R}\right)\left(e^{-6\pi R} - 2e^{-8\pi R} + e^{-10\pi R}\right)\right], & m = \pm 1 \\ P\sigma^2\left(\frac{2 - e^{-2\pi R} + e^{2\pi R}}{64\pi^2R^2}\right)\left(2e^{-4\pi R|m|} - e^{-4\pi R(|m|+1)} - e^{-4\pi R(|m|-1)}\right), & m \neq 0, \pm 1 \end{cases} \tag{A-20}$$

$$R_{nn}(m) = \begin{cases} \sigma^4\left(\frac{\pi R}{2} - \frac{1}{8}(1 - e^{-4\pi R})\right), & m = 0 \\ \frac{\sigma^4}{16}\left(e^{-4\pi R(|m|-1)} + e^{-4\pi R(|m|+1)} - 2e^{-4\pi R|m|}\right), & m \neq 0 \end{cases} \tag{A-21}$$

where $\sigma^2 = N_0/2T$ and $R = BT$ is the ratio of the arm filter 3-dB bandwidth B to the data rate, $1/T$. Note that, as $R \to \infty$, $R_{ss}(m) \to 0$ as expected. In this case, the data pulses approach the unfiltered case and consequently, the self-noise power approaches zero. In the limit $R \to \infty$, $R_{sn}(m) \to P\sigma^2$, which is the signal–noise power at the output of the integrate-and-dump filter when the input is white noise with spectral level $PN_0/2$ watts^2/Hz. Finally, $R_{nn}(m) \to \infty$ as $R \to \infty$, since in this case the input is white noise with spectral level $N_0^2\pi B/2$, which becomes unbounded as $R \to \infty$, $R = BT$, for fixed T.

Appendix B
Computing $\tilde{d}^2(t)$ in Eq. (A-1)

The data sequence $d(t)$, which is given mathematically by Eq. (2), has its Fourier transform given by

$$D(\omega) = \sum_{k=-\infty}^{\infty} d_k P(\omega) e^{-jk\omega T} \tag{B-1}$$

where the binary symbols d_k are ± 1 with equal probability and $P(\omega)$ is the Fourier transform, denoted $\mathcal{F}\{\}$, of the baseband NRZ pulse $p(t)$. Applying Eq. (B-1) to Eq. (10) one obtains

$$\tilde{D}(\omega) = \sum_{k=-\infty}^{\infty} d_k \tilde{P}(\omega) e^{-jk\omega T} \tag{B-2}$$

where $\tilde{P}(\omega)$ is defined to be

$$\tilde{P}(\omega) = P(\omega) H(\omega + \Delta\omega) \tag{B-3}$$

As a result, $\tilde{d}(t) = \mathcal{F}^{-1}\{\tilde{D}(\omega)\}$ is given as

$$\tilde{d}(t) = \sum_{k=-\infty}^{\infty} d_k \tilde{p}(t - kT) \tag{B-4}$$

where $\tilde{p}(t)$ is the inverse Fourier transform of $\tilde{P}(\omega)$. From Eq. (B-4), the term $\tilde{d}^2(t)$ in Eq. (A-1) can be written as

$$\tilde{d}^2(t) = \sum_{k=-\infty}^{\infty} \tilde{p}^2(t - kT) + \sum_{k=-\infty}^{\infty} \sum_{\substack{l=-\infty \\ l \neq k}}^{\infty} d_k d_l \tilde{p}(t - lT) \tilde{p}(t - kT) \tag{B-5}$$

The first term in Eq. (B-5) is a periodic complex function with period T. Consequently, it can be represented by a Fourier series:

$$\sum_{k=-\infty}^{\infty} \tilde{p}^2(t - kT) = \sum_{n=-\infty}^{\infty} C_n e^{j(2n\pi t/T)} \tag{B-6}$$

where the Fourier coefficients C_n are given by

$$C_n = \frac{1}{T} \mathcal{F}\{\tilde{p}^2(t)\}_{\omega = n(2\pi/T)} \tag{B-7}$$

For a one-pole filter, $\tilde{p}(t)$ can be computed to be

$$\tilde{p}(t) = \frac{\omega_B}{\omega_B + j\Delta\omega} \left(p(t) - e^{-(\omega_B + j\Delta\omega)t} u(t) + e^{-(\omega_B + j\Delta\omega)(t-T)} u(t - T) \right) \tag{B-8}$$

where ω_B is the 3-dB filter bandwidth in radians, $p(t) = u(t) - u(t - T)$, and $u(t)$ is the unit step function. Applying Eq. (B-8) to Eq. (B-7), the Fourier coefficients C_n as a function of $\Delta\omega T$ and $R = BT$ are computed to be

$$C_n(R) = \left(\frac{1}{1+j\frac{\Delta\omega T}{2\pi R}}\right)^2 \left((-1)^n \frac{\sin n\pi}{n\pi} - \frac{1}{2\pi R}\frac{\left(1+j\frac{\Delta\omega T}{2\pi R}\right)\left(1-e^{-(2\pi R+j\Delta\omega T)}\right)}{\left(1+j\frac{2n\pi+\Delta\omega T}{2\pi R}\right)\left(1+j\frac{n\pi+\Delta\omega T}{2\pi R}\right)}\right) \tag{B-9}$$

Note that for the special cases of $\Delta\omega = 0$ and $\Delta\omega = (-n\pi)/T$, Eq. (B-9) reduces to Table 2 of [9]. Additionally, for $n = 0$, Eq. (B-9) reduces to

$$C_0(R) = \left(\frac{1}{1+j\frac{\Delta\omega T}{2\pi R}}\right)^2 \left(1 - \frac{1}{2\pi R}\frac{1-e^{-(2\pi R+j\Delta\omega T)}}{1+j\frac{\Delta\omega T}{2\pi R}}\right) \tag{B-10}$$

Appendix C

Computing $R'_{ss}(\tau)$, $R'_{sn}(\tau)$, $R'_{nn}(\tau)$ and $R_{ss}(m)$, $R_{sn}(m)$, $R_{nn}(m)$

When applicable, the derivations that follow assume that the frequency error $\Delta f = 0$. This greatly simplifies the computation of the various autocorrelation functions and is not expected to change appreciably the final result of the main text. The reason for this is that all the significant noise components give rise to continuous spectra whose shapes are not expected to change much with Δf when $\Delta f \ll 1/T$. Furthermore, when computing $R'_{ss}(\tau)$, the second term in Eq. (A-7) is not included. This approximation is made because, except for the first harmonic which has a line component at $1/T \pm 2\Delta f$, the remaining harmonics give rise to line components far beyond the band of frequencies within which the error signal is expected. Additionally, power in the first harmonic which is at least 8 dB down from the component at $2\Delta f$ when $\Delta\omega T \leq 0.1$, is suppressed even further by the integrate-and-dump filter response preceding the FFT operation.

I. $R'_{ss}(\tau)$ and $R_{ss}(m)$

The self-noise $n'_{ss}(t)$ is given by Eq. (A-7). When $\Delta\omega = 0$, $\tilde{p}(t)$ is real, and $n'_{ss}(t)$ reduces to

$$n'_{ss}(t) = \frac{P}{2}\left(\sum_{k=-\infty}^{\infty}\sum_{\substack{l=-\infty \\ l\neq k}}^{\infty} d_k d_l \tilde{p}(t-lT)\tilde{p}(t-kT)\right)\sin 2\phi \tag{C-1}$$

where d_n is ± 1 at random with probability one-half, and ϕ, which is independent of d_n, is a uniform random variable in the interval $[0, 2\pi]$. The filtered pulse $\tilde{p}(t)$ is given by Eq. (B-8). The autocorrelation function of $n'_{ss}(t)$ is given by

$$R'_{ss}(\tau) = \mathcal{E}[n'_{ss}(t)n'_{ss}(t+\tau)] = \frac{P^2}{8}R(\tau) \tag{C-2}$$

where, after noting that $\mathcal{E}[\sin^2\phi] = \frac{1}{2}$, $R(\tau)$ can be defined as follows:

$$R(\tau) = \sum_{k=-\infty}^{\infty}\sum_{\substack{l=-\infty \\ l\neq k}}^{\infty}\sum_{m=-\infty}^{\infty}\sum_{\substack{n=-\infty \\ n\neq m}}^{\infty} d_k d_l d_m d_n \tilde{p}(t-kT)\tilde{p}(t-lT)\tilde{p}(t-mT)\tilde{p}(t-nT) \tag{C-3}$$

The function above, which is in general difficult to compute because the filtered pulse $\tilde{p}(t)$ is not time limited, can be approximated as follows. One begins by expressing $R(\tau)$ as the inverse Fourier transform of its corresponding spectral density.

$$R(\tau) = \int_{-\infty}^{\infty} S(\omega)e^{j\omega\tau}\frac{d\omega}{2\pi} \approx S(0)\lim_{\omega\to\infty}\int_{-\omega}^{\omega} e^{j\omega\tau}\frac{d\omega}{2\pi} \tag{C-4}$$

From Chapter 5 of [6], the dc component of the spectral density in Eq. (C-4) is given by

$$S(0) = 4T\sum_{l=1}^{\infty} R_d^2(lT) \tag{C-5}$$

where

$$R_d(lT) = \int_{-\infty}^{\infty} S_d(\omega)|H(\omega)|^2 e^{-j\omega lT}\frac{d\omega}{2\pi} \tag{C-6}$$

where $S_d(\omega)$ is the spectral density of the random NRZ data and $|H(\omega)|^2$ is the squared magnitude of the one-pole filter with 3-dB bandwidth B Hz. Grouping the exponential in the above integral with $|H(\omega)|^2$ and applying Parseval's theorem gives the corresponding integral in the transformed domain. Namely,

$$R_d(lT) = \int_{-T}^{T} \left(1 - \frac{|\tau|}{T}\right) \pi B e^{-2\pi B|\tau + lT|} d\tau = \frac{e^{-2\pi Rl}}{2\pi R} \left(-1 + \frac{e^{-2\pi R} + e^{2\pi R}}{2}\right) \tag{C-7}$$

where the parameter $R = BT$. Finally, $R'_{ss}(\tau)$ in Eq. (A-11) follows after back-substituting the last result.

The discrete autocorrelation function given by Eq. (A-19), which is the correlation function of the noise sequence $n_{ss}(n)$ given by Eq. (A-16), follows directly upon evaluating the next equation:

$$R_{ss}(m) = \frac{1}{T^2} \int_0^T \int_{mT}^{(m+1)T} R'_{ss}(|t_2 - t_1|) dt_2 dt_1 \tag{C-8}$$

where $R'_{ss}(\tau)$ is given by Eq. (A-11).

II. $R'_{sn}(\tau)$ and $R_{sn}(m)$

The signal–noise process $n'_{sn}(t)$ is given by Eq. (A-8). For $\Delta\omega = 0$, $\tilde{p}(t)$ is real and $n'_{sn}(t)$ reduces to

$$n'_{sn}(t) = \left(\sqrt{P} \sum_{k=-\infty}^{\infty} d_k \tilde{p}(t - kT) \cos\phi\right) \tilde{n}_q(t) + \left(\sqrt{P} \sum_{k=-\infty}^{\infty} d_k \tilde{p}(t - kT) \sin\phi\right) \tilde{n}_i(t) \tag{C-9}$$

Since the data and noise processes are independent of each other, the autocorrelation of the signal–noise product is the product of the autocorrelation of the individual signal and noise processes. Hence,

$$R'_{sn}(\tau) = \mathcal{E}[n'_{sn}(t) n'_{sn}(t + \tau)] = P R_s(\tau) R_n(\tau) \tag{C-10}$$

where

$$R_s(\tau) = \mathcal{E}\left[\sum_{k=-\infty}^{\infty} \sum_{l=-\infty}^{\infty} d_k d_l \tilde{p}(t - kT) \tilde{p}(t - lT)\right] \tag{C-11}$$

$$R_n(\tau) = \mathcal{E}[\tilde{n}_i(t) \tilde{n}_i(t + \tau)] = \mathcal{E}[\tilde{n}_q(t) \tilde{n}_q(t + \tau)] \tag{C-12}$$

The functions $R_s(\tau)$ and $R_n(\tau)$ are the autocorrelation functions of signal and noise processes at the output of a one-pole filter when the input signal process is random NRZ data, and the input noise process is white noise. Consequently, writing $R_s(\tau)$ as the inverse Fourier transform of its corresponding spectral density in terms of the input spectral density times the squared magnitude of the one-pole filter, grouping the exponential with the squared magnitude of the filter transfer function, and applying Parseval's theorem yields

$$R_s(\tau) = \int_{-T}^{T} \left(1 - \frac{|\tau'|}{T}\right) \frac{\pi B}{2} e^{-2\pi B|\tau' + \tau|} d\tau' \tag{C-13}$$

where B Hz is the 3-dB bandwidth of the one-pole filter. The noise correlation is well known to be

$$R_n(\tau) = \frac{N_0}{2} \pi B e^{-2\pi B|\tau|} \tag{C-14}$$

Finally, the signal–noise correlation given by Eq. (A-12) follows after substituting Eqs. (C-13) and (C-14) into Eq. (C-10).

The discrete autocorrelation function given by Eq. (A-20), which is the correlation function of the noise sequence $n_{sn}(n)$, is obtained upon evaluating the next equation:

$$R_{sn}(m) = \frac{1}{T^2} \int_0^T \int_{mT}^{(m+1)T} R'_{sn}(|t_2 - t_1|) dt_2 dt_1 \tag{C-15}$$

Since the integrand above depends only on the absolute difference $|t_2 - t_1|$, the double integral above can be reduced to the following simpler single integrals when $m = 0, 1, -1$. Namely,

$$\int_0^T \int_{mT}^{(m+1)T} R'_{sn}(|t_2 - t_1|) dt_2 dt_1 = \begin{cases} \int_{-T}^{T} R'_{sn}(|\tau|)(T - |\tau|) d\tau, & m = 0 \\ \\ \int_0^{2T} R'_{sn}(|\tau|) \tau d\tau, & m = 1, -1 \end{cases} \tag{C-16}$$

When $|m| > 1$, Eq. (C-15) reduces to the product of two single integrals in a straightforward manner.

III. $R'_{nn}(\tau)$ and $R_{nn}(m)$

The noise process $n'_{nn}(t)$ given by Eq. (A-9) is the product of the filtered inphase and quadraphase noise processes, $\tilde{n}_i(t)$ and $\tilde{n}_q(t)$. The autocorrelation of these noises, denoted by $R_n(\tau)$, is given by Eq. (C-14). Furthermore, since $\tilde{n}_i(t)$ and $\tilde{n}_q(t)$ are independent with respect to each other, $R_{nn}(\tau) = R_n^2(\tau)$ and Eq. (A-13) follows. The discrete autocorrelation $R_{nn}(m)$ is given upon evaluating the following equation:

$$R_{nn}(m) = \int_0^T \int_{mT}^{(m+1)T} R'_{nn}(|t_2 - t_1|) dt_2 dt_1 \tag{C-17}$$

where, when $m = 0$, the double integral above can be transformed to the following simpler single integral:

$$\int_0^T \int_0^T R'_{nn}(|t_2 - t_1|) dt_2 dt_1 = \int_{-T}^{T} R'_{nn}(|\tau|)(T - |\tau|) d\tau \tag{C-18}$$

When $m \neq 0$, Eq. (C-17) reduces to the product of two single integrals.

References

[1] S. Hinedi, "A Functional Description of the Advanced Receiver," *TDA Progress Report 42-100*, vol. October–December 1989, Jet Propulsion Laboratory, Pasadena, California, pp. 131–149, February 15, 1990.

[2] B. Shah and S. Hinedi, "A Comparison of Open-Loop Suppressed-Carrier Acquisition Techniques," *TDA Progress Report 42-103* , vol. July–September 1990, Jet Propulsion Laboratory, Pasadena, California, pp. 170–188, November 15, 1990.

[3] S. Aguirre, "Acquisition Times of Carrier Tracking Sampled Data Phase-Locked Loops," *TDA Progress Report 42-84*, vol. October–December 1985, Jet Propulsion Laboratory, Pasadena, California, pp. 88–93, February 15, 1986.

[4] S. Hinedi and B. Shah, "QPSK Carrier-Acquisition Performance in the Advanced Receiver II," *TDA Progress Report 42-100*, vol. October–December 1989, Jet Propulsion Laboratory, Pasadena, California, pp. 150–159, February 15, 1990.

[5] D. C. Rife and R. R. Boorstyn, "Single-Tone Parameter Estimation From Discrete-Time Observations," *IEEE Trans. Info. Theory*, vol. IT-20, no. 5, pp. 591–598, September 1974.

[6] A. V. Oppenheim and R. W. Schafer, *Discrete-Time Signal Processing*, New Jersey: Prentice-Hall, 1989.

[7] J. K. Holmes, *Coherent Spread Spectrum Systems*, New York: John Wiley & Sons, 1982.

[8] F. M. Gardner, *Phase Lock Techniques*, 2nd edition, New York: John Wiley & Sons, 1979.

[9] G. Hedin, J. K. Holmes, W. C. Lindsey, and K. T. Woo, "False Lock Phenomenon in Costas and Squaring Loops," *Proc. 1977 National Telecommunications Conference*, pp. 30:1-1–30:1-5, Los Angeles, California, 1977.